Heavy quark pair production in high energy pA collisions: Open heavy flavors

Hirotsugu Fujii and Kazuhiro Watanabe

September 3, 2018

Institute of Physics, University of Tokyo,
Komaba 3-8-1, Tokyo 153-8902, Japan

Abstract

We study open heavy flavor meson production in proton-nucleus (pA) collisions at RHIC and LHC energies within the Color Glass Condensate framework. We use the unintegrated gluon distribution at small Bjorken's x in the proton obtained by solving the Balitsky-Kovchegov equation with running coupling correction and constrained by global fitting of HERA data. We change the initial saturation scale of the gluon distribution for the heavy nucleus. The gluon distribution with McLerran-Venugopalan model initial condition is also used for comparison. We present transverse momentum spectra of single D and B productions in pA collisions, and the so-called nuclear modification factor. The azimuthal angle correlation of open heavy flavor meson pair is also computed to study the modification due to the gluon saturation in the heavy nucleus at the LHC.

1 Introduction

Heavy quark production in high-energy proton-nucleus (pA) collisions at RHIC and the LHC provides us with a unique opportunity to investigate the so-called *parton saturation* phenomenon[1, 2] at small Bjorken's x in the incoming nucleus. The large charm quark mass allows perturbative calculation of the quark production from the gluons, while high center-of-mass collision energy $\sqrt{s}$ makes the relevant x of the gluons still small. These low-x gluons are abundantly generated from the larger-x partons in view of the x evolution. Then the saturation momentum scale $Q_s^2(x)$ emerges dynamically as a semi-hard scale below which virtuality $(Q^2 < Q_s^2(x))$ coherence and nonlinearity of the x evolution become important. This dynamics of small-x degrees of freedom in hadrons is described with the Color Glass Condensate (CGC) effective theory [3].

The saturation scale $Q_{sA}^2(x)$ in a heavy nucleus of the atomic mass number A is enhanced by the larger valence color charges seen at moderate value of $x = x_0$. Indeed,

the empirical formula [4, 5] $Q_{sA}^2(x) = Q_{s0}^2 A^{1/3}(x_0/x)^\lambda$ with $Q_{s0}^2 = 0.2\,\text{GeV}^2$, $x_0 = 0.01$ and $\lambda = 0.3$ suggests that the saturation scale is already comparable to the charm quark mass $m_c \sim 1.5\,\text{GeV}$ with $A = 200$ at RHIC energy $\sqrt{s} = 200\,\text{GeV}$. Therefore quantitative analysis of particle production in pA collisions will be very crucial[6].

In the previous paper [7] we studied J/ψ and $\Upsilon(1S)$ productions in pA collisions within the CGC framework[8, 9], in order to quantify the effects of gluon saturation in a heavy nucleus on the heavy quark pair production. We extend here our study to the production of open heavy flavor mesons in pA collisions and will evaluate D and B production cross-sections differential in transverse momentum at mid and forward rapidities, and azimuthal correlations of the $D\bar{D}$ pair ($B\bar{B}$ pair as well). In the CGC framework, multiple scatterings and gluon merging dynamics are encoded in the effective unintegrated gluon distribution (uGD) function of a heavy nucleus. These effects will cause relative depletion of quark production yields and azimuthal momentum imbalance between the produced quark and antiquark. They will be more prominent in the momentum region lower than $Q_s^2(x)$.

This study is significant also in the context of nucleus-nucleus (AA) collisions as a benchmark for discriminating the initial nuclear effects from the subsequent hot-medium effects on heavy meson production, presuming that no hot medium is formed in pA collisions. Heavy flavor production in AA collisions measured at RHIC [10, 11] and the LHC [12, 13] shows a strong suppression (compared to that in pp collisions with appropriate normalization), similar in magnitude to that of light hadrons, which is interpreted as a large energy loss of the heavy quark in a hot medium [14, 15, 16, 17, 18]. Initial nuclear effects should be accounted properly here for precise evaluation of the medium effects.

Although azimuthal angle correlation measurement for charmed meson pair is inaccessible at RHIC so far due to limited statistics, LHCb collaboration recently measured the angle correlation at forward rapidity in pp collisions [19, 20]. We expect that it will become also available in AA collisions at the LHC. In AA collisions, the interactions of the heavy quarks with the hot medium will distort the angle correlation of the pair and may generate a new correlation by collective flow[21]. For a precise evaluation, again, we need to take account of the initial state effects.

We use the quark pair production formula obtained in Ref. [8, 9] at LO in the strong coupling constant α_s and the color charge density ρ_p in the proton, but including all orders in the color charge density ρ_A in the nucleus. In the large N limit, we only need the three point function $\phi^{q\bar{q},g}$ of the gluons in the nuclear target. We assume that $\phi^{q\bar{q},g}$ can be obtained from the dipole amplitude S, which seems also valid in the large N.

It is now standard to use non-linear Balitsky-Kovchegov (BK) equation [22, 23] for describing the x dependence of the uGD in a hadron. It is argued that the inclusion of running coupling corrections to the BK equation (now called rcBK equation) is essential to phenomenology[24, 25, 26]. Indeed, the rcBK equation with an appropriate initial condition can fit the HERA DIS data quite well [27, 28] and are successful in reproducing/predicting the data at hadron colliders quantitatively [29, 30, 31, 32]. We use the numerical solution of the rcBK equation to describe the x dependence of the gluon distribution in the nuclear target in the present work in the same way as in our previous

paper[7].

This paper is organized as follows. In Sec. 2 we briefly introduce the expression for production cross-section of open heavy flavor mesons in pA collisions within the CGC framework, and the unintegrated gluon distribution obtained by solving the rcBK equation. Next in Sec. 3 we present numerical results for single open heavy flavor production at RHIC and LHC energies, and also azimuthal angle correlation between the pair of heavy mesons. Summary is given in Sec. 4.

2 Heavy flavor meson production from CGC

Heavy quark pair production cross-section of a quark with transverse momentum $\boldsymbol{q}$ and rapidity y_q and an anti-quark with $\boldsymbol{p}$ and y_p is given to the leading order in α_s and ρ_p but full orders in ρ_A as [8, 9]

$$\frac{d\sigma_{q\bar{q}}}{d^2\boldsymbol{p}_\perp d^2\boldsymbol{q}_\perp dy_p dy_q} = \frac{\alpha_s^2 N}{8\pi^4(N^2-1)}\frac{1}{(2\pi)^2}\int\limits_{\boldsymbol{k}_{2\perp},\boldsymbol{k}_\perp} \frac{\Xi(\boldsymbol{k}_{1\perp},\boldsymbol{k}_{2\perp},\boldsymbol{k}_\perp)}{\boldsymbol{k}_{1\perp}^2\boldsymbol{k}_{2\perp}^2}\,\phi_{A,y_2}^{q\bar{q},g}(\boldsymbol{k}_{2\perp},\boldsymbol{k}_\perp)\,\varphi_{p,y_1}(\boldsymbol{k}_{1\perp})\,,$$

(1)

where

$$\begin{aligned}
\Xi(\boldsymbol{k}_{1\perp},\boldsymbol{k}_{2\perp},\boldsymbol{k}_\perp) =& \mathrm{tr}_{\mathrm{d}}\Big[(\slashed{q}+m)T_{q\bar{q}}(\slashed{p}-m)\gamma^0 T_{q\bar{q}}^\dagger\gamma^0\Big] \\
&+ \mathrm{tr}_{\mathrm{d}}\Big[(\slashed{q}+m)T_{q\bar{q}}(\slashed{p}-m)\gamma^0 T_g^\dagger\gamma^0 + \mathrm{h.c.}\Big] \\
&+ \mathrm{tr}_{\mathrm{d}}\Big[(\slashed{q}+m)T_g(\slashed{p}-m)\gamma^0 T_g^\dagger\gamma^0\Big]
\end{aligned}$$

(2)

represents the relevant hard matrix element squared, and transverse momentum conservation $\boldsymbol{k}_{1\perp}+\boldsymbol{k}_{2\perp}=\boldsymbol{p}_\perp+\boldsymbol{q}_\perp$ the parton level should be understood. Here index 1 (2) refers to the quantity on the proton (nucleus) side. We have used the notation $\int_{\boldsymbol{k}_\perp} \equiv \int d^2\boldsymbol{k}_\perp/(2\pi)^2$ for transverse momentum integration. The $T_{q\bar{q}}$ term corresponds to the process where the gluon from the proton splits into the quark-pair which then interacts with the gluons in the target nucleus, while the T_g term corresponds to the one where the gluon from the proton interacts with the gluons in the nucleus and then splits into the quark pair. The explicit expressions for $T_{q\bar{q}}$ and T_g can be found in [8, 9].

The quark pair production cross-section (1) involves the gluon 2-, 3- and 4-point functions of the heavy nucleus in general[8], but in the large-N limit we can express the cross-section with a single function $\phi_{A,y_2}^{q\bar{q},g}(\boldsymbol{k}_{2\perp},\boldsymbol{k}_\perp)$ in the form of Eq. (1). Furthermore, we have assumed the translational invariance in the transverse plane of the large nucleus, i.e., impact parameter dependence is simply ignored. Within this approximation, the 3-point function $\phi_{A,y_2}^{q\bar{q},g}(\boldsymbol{k}_{2\perp},\boldsymbol{k}_\perp)$ describes the gluon distribution in the nucleus and is expressed as[8, 9]

$$\phi_{A,Y}^{q\bar{q},g}(\boldsymbol{l}_\perp,\boldsymbol{k}_\perp) = \pi R_A^2\,\frac{N\boldsymbol{l}_\perp^2}{4\alpha_s}\,S_Y(\boldsymbol{k}_\perp)\,S_Y(\boldsymbol{l}_\perp-\boldsymbol{k}_\perp)\,,$$

(3)

3

where $S_Y(\boldsymbol{k}_\perp)$ is the Fourier-transformed dipole amplitude in the fundamental representation. The uGD of the nucleus is obtained by integrating over $\boldsymbol{k}_\perp$[8]:

$$\phi_{A,Y}^{g,g}(\boldsymbol{l}_\perp) = \int_{\boldsymbol{k}_\perp} \phi_{A,Y}^{q\bar{q},g}(\boldsymbol{l}_\perp, \boldsymbol{k}_\perp) \ . \tag{4}$$

The uGD $\varphi_{p,y}(\boldsymbol{k}_{1\perp})$ of the proton is obtained by replacing the transverse area πR_A^2 and the amplitude S_Y with those for the proton.

Single quark production cross-section is obtained by integrating the pair production cross-section (1) over the anti-quark phase space:

$$\frac{d\sigma_q}{d^2\boldsymbol{q}_\perp dy_q} = \int \frac{dp^+}{p^+} \, d^2\boldsymbol{p}_\perp \frac{d\sigma_{q\bar{q}}}{d^2\boldsymbol{p}_\perp d^2\boldsymbol{q}_\perp dy_p dy_q} \ . \tag{5}$$

Dividing the cross-section (1) or (5) with the total inelastic cross-section σ_{hadr}^{pA}, which we estimate as $\sigma_{hadr}^{pA} = \pi(R_A + R_p)^2 \approx \pi R_A^2$, we can obtain the average multiplicity per event[1]. If we compute the multiplicity per event, the total inelastic cross-section is effectively cancelled out with the transverse size of nucleus πR_A^2 in $\phi_{A,y_2}^{q\bar{q},g}(\boldsymbol{k}_{2\perp}, \boldsymbol{k}_\perp)$ and therefore the proton size only remains explicitly in the expression of multiplicity. We set the proton size as $R_p = 0.9$ fm throughout this paper.

Energy dependence of the cross-section is implicit in the gluon correlator $\phi_{A,Y}^{q\bar{q},g}(\boldsymbol{l}_\perp, \boldsymbol{k}_\perp)$, through the rapidity $Y = \ln(1/x)$ evolution of the dipole amplitude

$$S_Y(\boldsymbol{x}_\perp) \equiv \frac{1}{N} \mathrm{tr} \langle \widetilde{U}(\boldsymbol{x}_\perp) \widetilde{U}^\dagger(\boldsymbol{0}) \rangle_Y \ , \tag{6}$$

where $\widetilde{U}(\boldsymbol{x}_\perp)$ is the eikonal phase along the light-cone in the fundamental representation, and $\langle \cdot \rangle_Y$ indicates the average over the charge density distribution in the target at the scale Y. Physically, $S_Y(\boldsymbol{x})$ is the eikonal scattering matrix, probed by a quark-antiquark pair moving along the light-cone direction in the background gauge field in the target nucleus. The amplitude $S_Y(\boldsymbol{x})$ obeys the BK equation[22, 23]:

$$-\frac{d}{dY} S_Y(\boldsymbol{r}_\perp) = \int d\boldsymbol{r}_{1\perp} \, \mathcal{K}(\boldsymbol{r}_\perp, \boldsymbol{r}_{1\perp}) \left[S_Y(\boldsymbol{r}_\perp) - S_Y(\boldsymbol{r}_{1\perp}) S_Y(\boldsymbol{r}_{2\perp}) \right] \ , \tag{7}$$

where $\boldsymbol{r}_\perp = \boldsymbol{r}_{1\perp} + \boldsymbol{r}_{2\perp}$ and $\mathcal{K}(\boldsymbol{r}_\perp, \boldsymbol{r}_{1\perp})$ is the evolution kernel. The BK equation is closed in the 2-point function $S_Y(\boldsymbol{x})$, and therefore is numerically much easier to be handled.

It has been demonstrated [25, 26] that the BK equation with the running coupling corrections in Balitsky's prescription[24] but without the subtraction term (rcBK equation):

$$\mathcal{K}(\boldsymbol{r}_\perp, \boldsymbol{r}_{1\perp}) = \frac{\alpha_s(r^2)N}{2\pi^2} \left[\frac{1}{r_1^2} \left(\frac{\alpha_s(r_1^2)}{\alpha_s(r_2^2)} - 1 \right) + \frac{r^2}{r_1^2 r_2^2} + \frac{1}{r_2^2} \left(\frac{\alpha_s(r_2^2)}{\alpha_s(r_1^2)} - 1 \right) \right] \tag{8}$$

---

[1]The expression (1) is for *single* quark-pair production. Ref. [19] reports that double charm production amounts to 10 % of single charm production in forward region in pp collisions at $\sqrt{s} = 7$ TeV.

set	$Q^2_{s0,\mathrm{p}}/\mathrm{GeV}^2$	γ	α_{fr}	C
g1118	0.1597	1.118	1.0	2.47
MV	0.2	1	0.5	1

Table 1: Parameter values of the dipole amplitude. $\Lambda = 0.241$ GeV is fixed.

includes the important part of the NLO corrections. The behavior of the resultant saturation scale is compatible with HERA data: $Q^2_s(Y) \propto \exp(\lambda Y)$ with $\lambda \approx 0.3$ [4, 5, 26].

Global fit analysis of the compiled HERA e+p data at $x < x_0 = 0.01$ was performed in [27, 28] using the rcBK equation with the initial condition at $x = x_0$

$$S_{Y_0}(\boldsymbol{r}_\perp) = \exp\left[-\frac{(r^2 Q^2_{s0,\mathrm{p}})^\gamma}{4} \ln\left(\frac{1}{\Lambda r} + e\right)\right] . \tag{9}$$

Here, in the evolution, we modify the infrared regularization of the running coupling in the coordinate space to the smooth one[31]:

$$\alpha_s(r^2) = \left[b_0 \ln\left(\frac{4C^2}{r^2\Lambda^2} + a\right)\right]^{-1} \tag{10}$$

with $b_0 = 9/(4\pi)$. The constant a is introduced so as to freeze the coupling constant smoothly at $\alpha_s(r \to \infty) = \alpha_{fr}$. The parameter values are listed in Table 1. We also list a parameter set with the McLerran-Venugopalan (MV) model initial condition $\gamma = 1$, for comparison.

For a heavy nucleus A, the saturation scale at moderate values of x will be enhanced by a factor of the nuclear thickness $T_A(\boldsymbol{b})$. As we limit our analysis to mean bias events in this paper, we assume a simpler relation

$$Q^2_{s,A}(x_0) = A^{1/3} Q^2_{s,p}(x_0) . \tag{11}$$

We shall allow the saturation scale of the nucleus with $A = 200$ in the range $Q^2_{s,A} = (4 - 6) \times Q^2_{s,p}$ at initial point $x_0 = 0.01$. The 3-point function in the nucleus at $x < x_0$ can be obtained from the numerical solution of the rcBK equation via Eq. (3). For $x_0 \le x \le 1$, on the other hand, we apply the following phenomenological Ansatz [9]:

$$\phi^{q\bar{q},g}_{A,Y}(\boldsymbol{l}_\perp, \boldsymbol{k}_\perp) = \phi^{q\bar{q},g}_{A,Y_0}(\boldsymbol{l}_\perp, \boldsymbol{k}_\perp) \left(\frac{1-x}{1-x_0}\right)^4 \left(\frac{x_0}{x}\right)^{0.15} , \tag{12}$$

where $Y_0 \equiv \ln(1/x_0)$.

In the present paper we compute the heavy meson production in pA collsions. Heavy flavor meson pair production cross-section can be written as

$$\frac{d\sigma_{h\bar{h}}}{d^2\boldsymbol{q}_{h\perp}d^2\boldsymbol{q}_{\bar{h}\perp}dy_q dy_p} = f_{q\to h} f_{\bar{q}\to\bar{h}} \int\limits_{z_{1\min},z_{2\min}}^1 dz_1 dz_2 \frac{D^h_q(z_1)}{z_1^2} \frac{D^{\bar{h}}_{\bar{q}}(z_2)}{z_2^2} \frac{d\sigma_{q\bar{q}}}{d^2\boldsymbol{q}_\perp d^2\boldsymbol{p}_\perp dy_q dy_p} \tag{13}$$

5

Here $\boldsymbol{q}_{h\perp}$ ($\boldsymbol{q}_{\bar{h}\perp}$) and y_q ($y_{\bar{q}}$) are respectively transverse momentum and rapidity of the produced meson h ($\bar{h}$). The longitudinal momentum fraction z_1 (z_2) of the heavy meson fragmented from the heavy quark (anti-quark) is defined as $q_{h\perp} = z_1 q_\perp$ ($q_{\bar{h}\perp} = z_2 p_\perp$). The lower limit $z_{\min}$ is set by the momentum fraction of the meson fragmented from the heavy quark with the maximum $q_\perp$ allowed kinematically. Here we assume that the meson and the quark have the same rapidity, $y_q = y_h$ ($y_p = y_{\bar{h}}$).

For the fragmentation function $D(z)$, we use the Kartvelishvili fragmentation function[33],

$$D_q^h(z) = (\alpha + 1)(\alpha + 2)z^\alpha(1 - z) . \tag{14}$$

The value of α is set to 3.5 (13.5) for D (B) [34, 35]. The factor $f_{q \to h}$ represents the transition rate of the heavy quark q fragmenting into the heavy meson h. Empirical values, $f_{c \to D^0} = 0.565$, $f_{c \to D^{*+}} = 0.224$, and $f_{b \to \bar{B}^0} = 0.401$ are taken from [36, 37]. For the charge conjugate states, we assume $D_q^h(z) = D_{\bar{q}}^{\bar{h}}(z)$ and $f_{\bar{q} \to \bar{h}} = f_{q \to h}$.

Similarly single heavy meson production cross-section is expressed in convolution form of quark production cross-section (5) and the fragmentation function $D_q^h(z)$,

$$\frac{d\sigma_h}{d^2\boldsymbol{q}_{h\perp}dy} = f_{q \to h} \int\limits_{z_{\min}}^{1} dz \frac{D_q^h(z)}{z^2} \frac{d\sigma_q}{d^2\boldsymbol{q}_\perp dy} . \tag{15}$$

Again we set $q_{h\perp} = zq_\perp$ and $y_q = y_h = y$.

Finally it would be instructive to show the kinematical coverage of x variable in the heavy meson production at RHIC and LHC energies. We plot in Fig. 1 the $x_{1,2}$ distribution of single heavy meson production at a particular transverse momentum and rapidity. We find in Fig. 1 (a) that both x_1 and x_2 contributing to single charmed meson production at $p_\perp = 2$ GeV/c and $y = 0$ at $\sqrt{s} = 200$ GeV are larger than $x_0 = 0.01$, while at forward rapidity $y = 2$ the production gets sensitivity to small $x_2 < x_0$. In other words, the mid-rapidity production of single heavy mesons is sensitive to the initial $\phi_{A,Y0}^{\bar{q}q,g}$ and x-evolution effect shows up only at forward meson production at RHICh energy. However, it is seen in Fig. 1 (b) and (c) that at $\sqrt{s} = 5.02$ TeV small x gluons around 10^{-3} dominate the production even at mid rapidity. In the forward-rapidity production, the x_2 value of the gluons from the nucleus can become lower than 10^{-4}, where one would expect good sensitivity of heavy meson production to x-evolution and parton saturation. Even for bottomed meson production the situation is similar, as seen in Fig. 1 (d). Thus heavy quark productions, which may be evaluated with perturbation method, can be used to probe the small-x dynamics by studying the heavy meson production at lower $p_\perp$ and forward rapidity at the LHC.
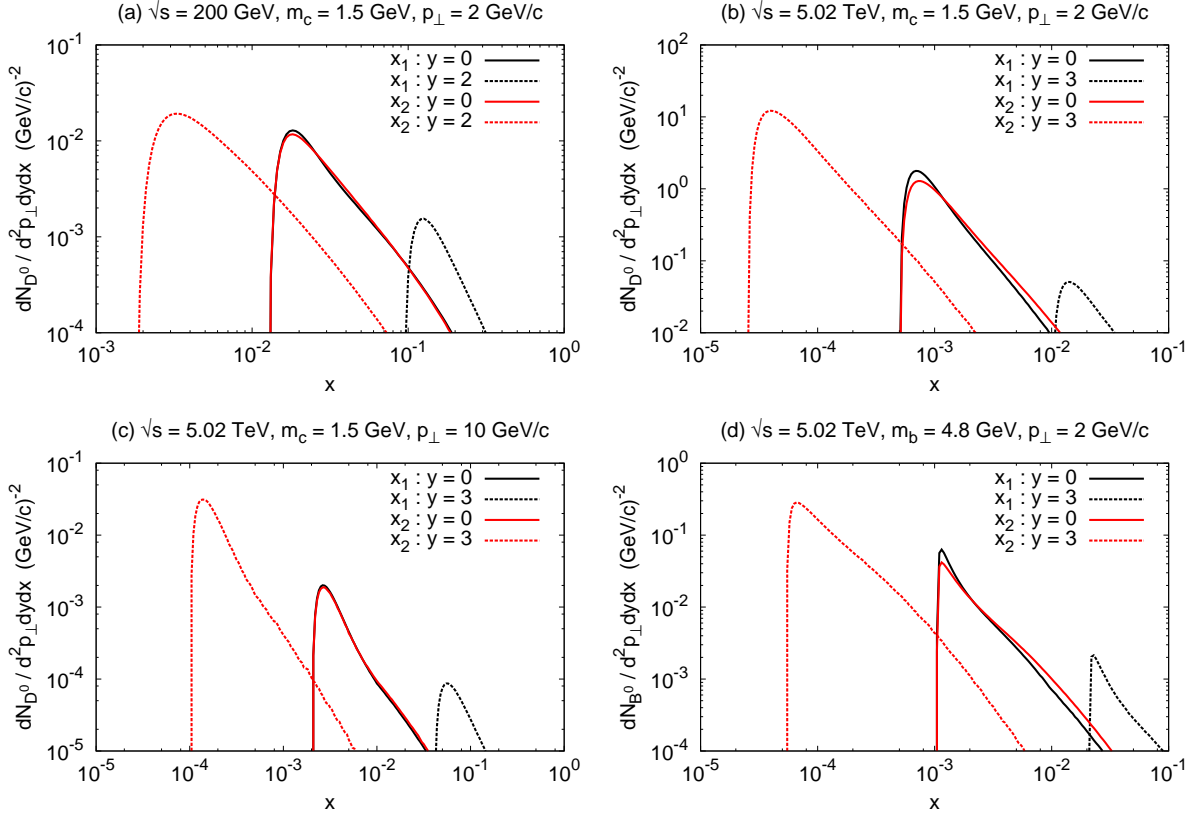
Figure 1: x_1 (black) and x_2 (red) coverages of D^0 production at mid and forward rapidities, for fixed $p_\perp = 2$ GeV at $\sqrt{s} = 200$ GeV (a), and for fixed $p_\perp = 2$ (b) and 10 GeV (c) at $\sqrt{s} = 5.02$ TeV. $x_{1,2}$ coverages of B^0 production are shown in (d) for fixed $p_\perp = 2$ at $\sqrt{s} = 5.02$ TeV.
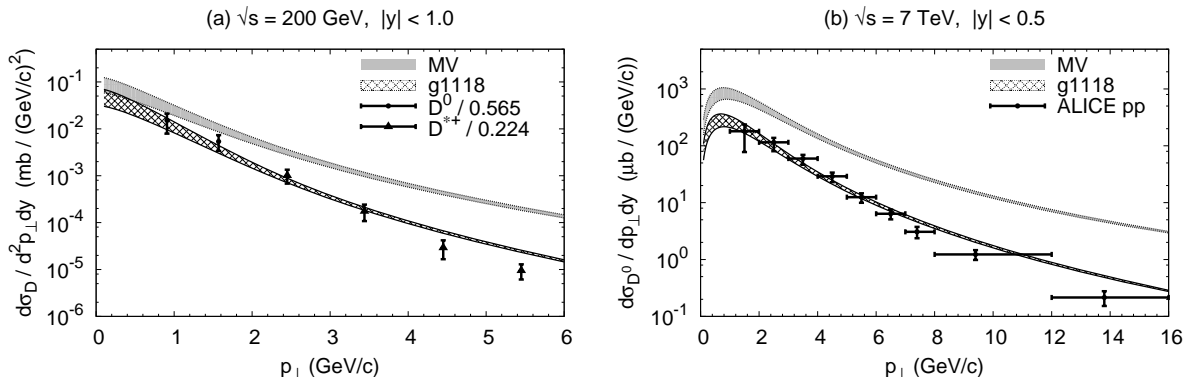
Figure 2: (a) Differential cross-section of D (rescaled as $D^0/f_{c\to D^0}$ and $D^{*+}/f_{c\to D^{*+}}$) vs transverse momentum $p_\perp$ for rapidity range $|y| < 1.0$ in pp collisions at $\sqrt{s} = 200$ GeV, computed with Eq. (15) with uGD sets MV (gray band) and g1118 (double-hatched). The upper (lower) curve of the band corresponds to the result with $m_c = 1.2$ (1.5) GeV. The data is taken from Ref. [40]. (b) Differential cross-section of D^0 vs transverse momentum $p_\perp$ at $|y| < 0.5$ in pp collisions at $\sqrt{s} = 5.02$ TeV. The ALICE data is taken from Ref. [38].

3 Numerical Results

In numerical calculations, we mainly use the uGD set g1118 in Table 1, and compare the results to those with set MV and available experimental data.

3.1 Transverse momentum spectrum

3.1.1 pp collisions

We study D meson production cross-section at mid rapidity in pp collisions at $\sqrt{s} = 200$ GeV and 5.02 TeV. Although the expression (15) is derived for a dilute-dense system such as pA, we apply it here by substituting the numerical solution for the proton into $\phi_{A,Y}^{q\bar{q},g}(\boldsymbol{l}_\perp, \boldsymbol{k}_\perp)$. By comparing the result with available data, we can examine the applicability of our formula. Furthermore we actually need the cross-sections in pp collisions as the normalization when we study the nuclear modification of the cross-sections in pA collisions.

We compute transverse momentum ($p_\perp$) spectrum of D meson production cross-section with uGD sets g1118 and MV in Table 1, and show the results in Fig. 2 together with the available data at $|y| < 1$ and at $\sqrt{s} = 200$ GeV[40] and at $|y| < 0.5$ and at $\sqrt{s} = 5.02$ TeV[38]. The upper (lower) curve of each band indicates the result with charm quark mass $m_c = 1.2$ (1.5) GeV. We find that $p_\perp$ dependence of D production is better described with uGD set g1118, although it gives still harder spectrum at high $p_\perp$.

Next we show forward B^0 production cross-section in $2 < y < 4.5$ in pp collisions at $\sqrt{s} = 5.02$ TeV as a function of $p_\perp$ in Fig. 3 (a) and the $p_\perp$-integrated cross-section as a
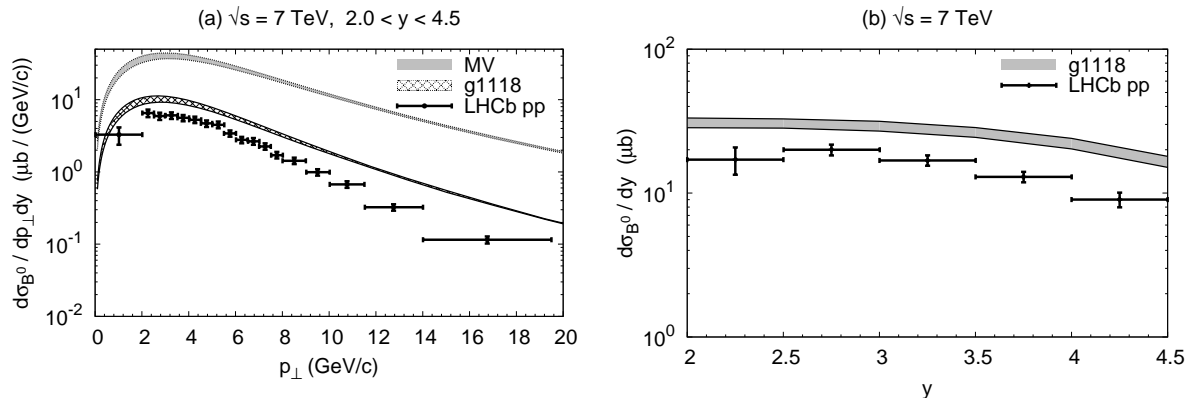
Figure 3: (a) Differential cross-section of B^0 vs transverse momentum $p_\perp$ for rapidity range $2 < y < 4.5$ in pp collisions at $\sqrt{s} = 5.02$ TeV, computed with Eq. (15) with uGD sets MV (gray band) and g1118 (double-hatched). The upper (lower) curve of the band corresponds to the result with $m_b = 4.5$ (4.8) GeV. (b) Differential cross-section of B^0 vs y in the range $0 < p_\perp < 40$ GeV in pp collisions at $\sqrt{s} = 5.02$ TeV. The notation of the curve is the same as in (a). The LHCb data is taken from Ref. [42].

function of y in Fig. 3 (b). The upper (lower) curve of each band indicates the result with the bottom quark mass $m_b = 4.5$ (4.8) GeV. The result with uGD set g1118 describes $p_\perp$ and y dependences of the data [42] better than that with set MV. But the magnitude of cross-section is larger than the data by about a factor of $2 - 3$. We comment here that large-x_1 gluons in the proton become relevant in B^0 production at forward rapidity and/or at high $p_\perp$. Therefore the numerical result is sensitive to the extrapolation Ansatz Eq. (12) of the uGD for large x.

3.1.2 pA collisions

We plot in Fig. 4 (a) the transverse momentum spectrum of D^0 multiplicity in the rapidity range $|y| < 1.0$ in pA collisions at $\sqrt{s} = 200$ GeV. We choose the initial saturation scale of the uGD in the heavy nucleus as $Q_{s0,A}^2(x = x_0) = 6Q_{s0,p}^2$. The upper (lower) curve of the bands indicate the result with $m_c = 1.2$ (1.5) GeV. We find that the results obtained with sets g1118 and MV fairly describe the available data at low $p_\perp \lesssim 2$ GeV [41] although high-$p_\perp$ behaviors are different. We show in Fig. 4 (b) D^0 production spectrum in $-1 < y < 0$ at $\sqrt{s} = 5.02$ TeV [2]. The uGD sets MV and g1118 give different $p_\perp$ dependences of the D meson spectrum: Set MV yields harder $p_\perp$ spectrum.
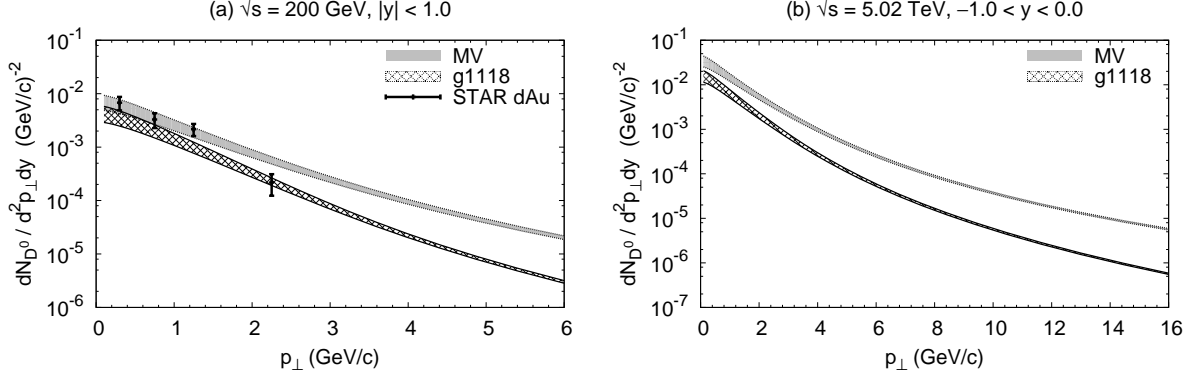
Figure 4: Transverse momentum spectrum of D^0 multiplicity per event in pA collisions, computed with Eq. (15) with uGD sets MV (gray) and g1118 (double-hatch), in rapidity range $|y| < 1.0$ at $\sqrt{s} = 200$ GeV (a) and in $-1.0 < y < 0.0$ at $\sqrt{s} = 5.02$ GeV (b). The upper (lower) curve of the band corresponds to the result with $m_c = 1.2$ (1.5) GeV. dAu data is taken from [41].
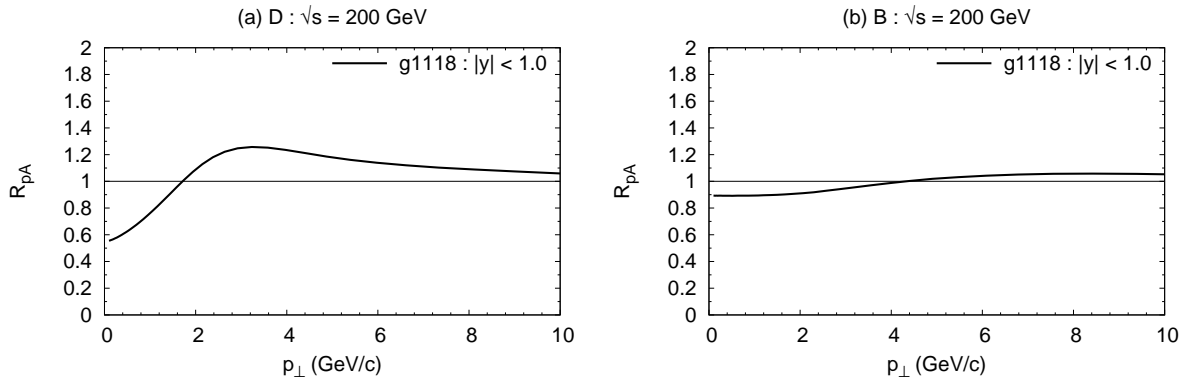

Figure 5: (a) Nuclear modification factor R_{pA} of D production vs $p_\perp$ computed with Eq. (16) with uGD set g1118 with $m_c = 1.5$ GeV in the rapidity range $|y| < 1.0$ at $\sqrt{s} = 200$ GeV. (b) $R_{\mathrm{pA}}(p_\perp)$ of B production with $m_b = 4.8$ GeV.
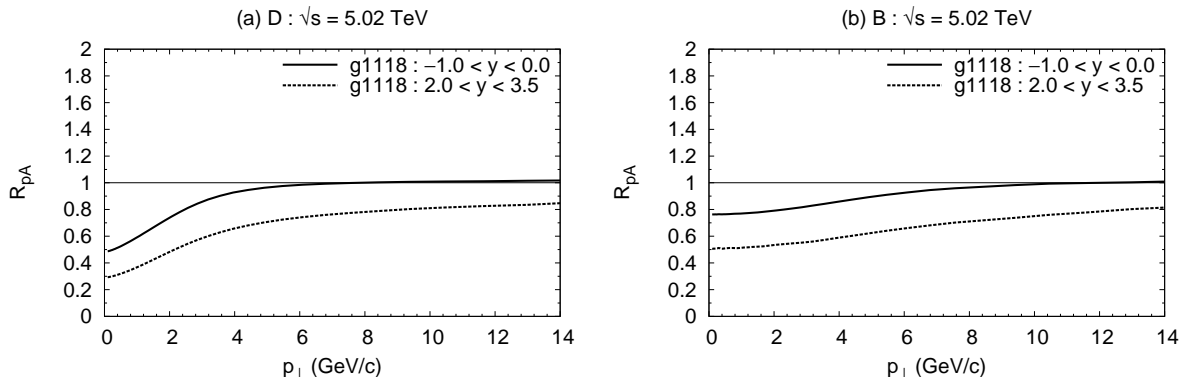
10

Figure 6: Nuclear modification factor $R_{\mathrm{pA}}(p_\perp)$ of (a) D and (b) B productions for $-1 < y < 0$ (solid line) and $2 < y < 3.5$ (dotted line) at $\sqrt{s} = 5.02$ TeV.

3.2   Transverse momentum dependence of R_{pA}

Now let us discuss the nuclear modification factor for pA collisions defined as

$$R_{\mathrm{pA}} = \frac{dN_h/d^2p_\perp dy\big|_{\mathrm{pA}}}{N_{\mathrm{coll}}\ dN_h/d^2p_\perp dy\big|_{\mathrm{pp}}}\ . \tag{16}$$

Here we set the number of binary nucleon-nucleon collisions to $N_{\mathrm{coll}} = A^{\gamma/3}$[32, 7]. Model uncertainties in our calculation will largely cancel out in the ratio of multiplicity per event in pA collisions to that in pp collisions.

In Fig. 5 we plot R_{pA} of (a) D and (b) B productions as a function of $p_\perp$ at mid rapidity ($|y| < 1.0$) at $\sqrt{s} = 200$ GeV. We use the uGD set g1118 in this subsection. We have checked that R_{pA} is insensitive to the variation of the heavy quark mass within the range considered here, and we show the results with $m_c = 1.5$ GeV for D production and $m_b = 4.8$ GeV for B production.

The nuclear modification factor R_{pA} of D production is suppressed at lower $p_\perp \lesssim 2$ GeV while enhanced at higher $p_\perp \gtrsim 2$ GeV. As seen in Fig. 1 (a), heavy mesons are produced from the gluons with moderate values of x, whose distribution is determined by the initial condition for ϕ_A. Thus the suppression and enhancement of R_{pA} can be interpreted as the effects of the multiple scatterings in the nucleus encoded in ϕ_A. On the other hand, R_{pA} of B production in Fig. 5 (b) shows little structure as a function $p_\perp$. This is because the larger bottom mass suppresses the effects of multiple scatterings, i.e., $Q^2_{A,y0}/m_b^2 \ll 1$. That is, B production scales with N_{coll} at RHIC energy.

Next, we study the nuclear modification R_{pA} of D and B productions at $\sqrt{s} = 5.02$ TeV. R_{pA} of D production shown in Fig. 6 (a) indicates that there is a strong suppression at lower $p_\perp$ and that no Cronin-like peak structure is seen at mid rapidity ($-1 < y < 0$) by

---

[2]Rapidity in the center-of-mass frame in pA collisions at $\sqrt{s} = 5.02$ TeV is shifted by $\Delta y = 0.465$ from that in the laboratory frame.
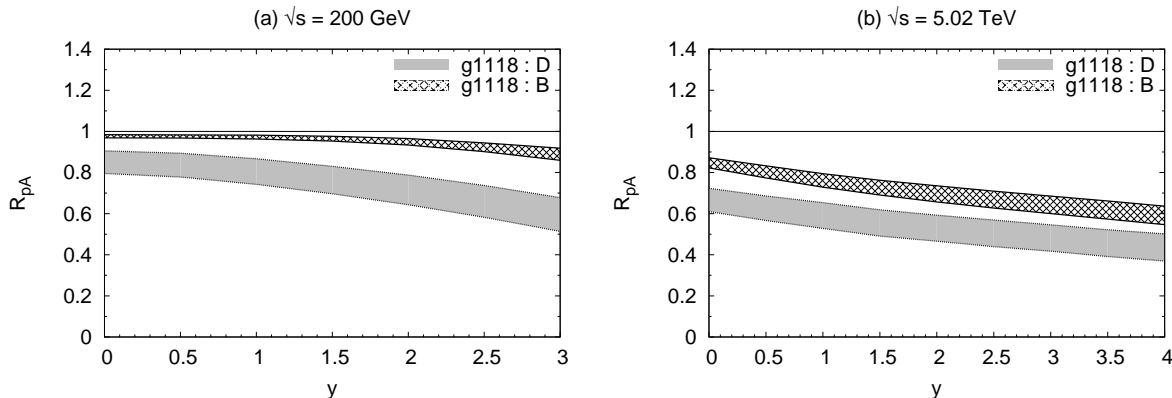
Figure 7: Nuclear modification factor R_{pA} for D (gray) and B (double-hatched) vs rapidity y in pA collisions at (a) $\sqrt{s} = 200$ GeV and (b) $\sqrt{s} = 5.02$ TeV. The uGD set g1118 is used. The bands indicate uncertainties from the variations $m_c = 1.2 - 1.5$ GeV for D, and $m_b = 4.5 - 4.8$ GeV for B and also $Q^2_{s0,A} = (4 - 6)Q^2_{s0,p}$.

the quantum x-evolution effects on the small x_2 gluons. We see the stronger suppression of R_{pA} in the wider range of $p_\perp$ at forward rapidity $(2 < y < 3.5)$, compared to that at mid rapidity. At $\sqrt{s} = 5.02$ TeV, B production at low $p_\perp$ shows a suppression similar to but weaker than the D production as shown in Fig. 6 (b).

3.3 Rapidity dependence of R_{pA}

The nuclear modification factor $(R_{\text{pA}}(y))$ of the heavy meson multiplicities dN/dy in pA collisions as a function of y provides important information about how the saturation effect evolves as moving to forward rapidity region. In Fig. 7 shown are the R_{pA} of D (gray band) and B (double hatched band) mesons as a function of rapidity at $\sqrt{s} = 200$ GeV (a) and 5.02 TeV (b).

We have allowed the variation of the initial saturation scale at $x = x_0$ in the heavy nucleus as $Q^2_{s0,A}(x = x_0) = (4 - 6)Q^2_{s0,p}$ with $A^{1/3} = 4 - 6$ here. The upper (lower) curve of the band of D production in Fig. 7 now corresponds to the result with $m_c = 1.5$ (1.2) GeV and $A^{1/3} = 4$ (6). For B production, the upper (lower) curve corresponds to the result obtained with $m_b = 4.8(4.5)$ GeV and $A^{1/3} = 4(6)$. The width of the band here comes mainly from the change of $A^{1/3} = 4 - 6$.

We find in Fig. 7 (a) that R_{pA} of the D production at mid rapidity at $\sqrt{s} = 200$ GeV is suppressed, which reflects the multiple scattering effect as we have discussed in Fig. 5. Stronger suppression of D production is seen with increasing the rapidity, in accord with the quantum evolution of the gluon distribution ϕ_A. On the other hand, for B production, R_{pA} shows no appreciable change with the increasing rapidity at RHIC energy, besides a subtle suppression at very forward rapidities.

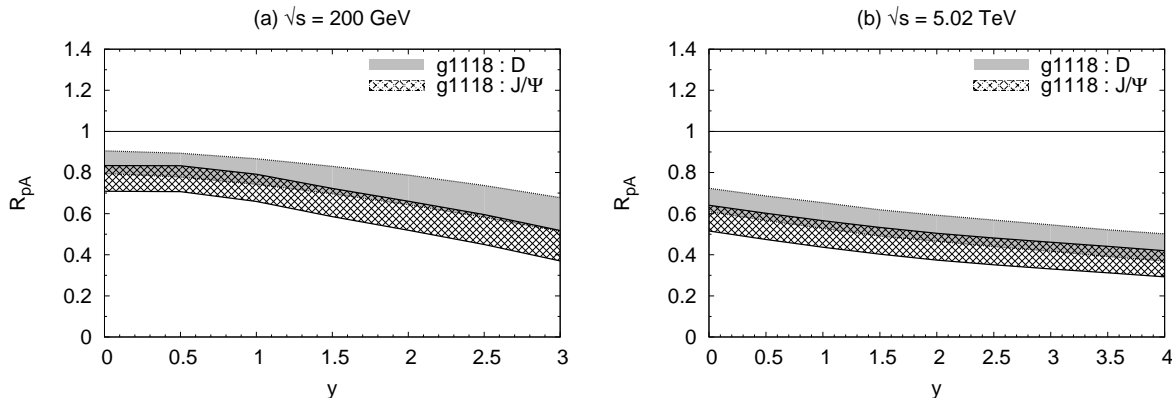At $\sqrt{s} = 5.02$ TeV, R_{pA} of both D and B productions show large depletions even

Figure 8: Nuclear modification factor R_{pA} for D and J/ψ vs y in pA collisions at (a) $\sqrt{s} = 200$ GeV and (b) $\sqrt{s} = 5.02$ TeV. The bands indicate the uncertainties from the variations $m_c = 1.2 - 1.5$ GeV and $Q^2_{s0,A} = (4 - 6)Q^2_{s0,p}$.

at mid rapidity as seen in Fig. 7 (b). Since the large colliding energy of the LHC gives rise to much smaller $x_2 < x_0$ of participating gluons (Fig. 1 (b)–(d)), small-x effects have already become relevant at mid rapidity, and even B production shows a suppression with increasing rapidity.

Finally we compare R_{pA} for D and J/ψ productions as a function of rapidity at (a) $\sqrt{s} = 200$ GeV and (b) $\sqrt{s} = 5.02$ TeV in Fig. 7. We compute the J/ψ production using color evaporation model, where the heavy quark pair produced below the $D\bar{D}$ threshold is assumed to bound into the quarkonium state with a fixed probability irrespective of the pair's color states. (See Ref. [7] for details). We notice that J/ψ production is more suppressed than D meson. This is because, in addition to the saturation effects of the initial gluons, the produced quark pair experiences the multiple scatterings with the gluons in the target. This effect increases the invariant mass of the pair on average. In the color evaporation model, if the quark pair is kicked beyond the invariant mass threshold, it cannot bound into the quarkonium, which results in a stronger suppression of the quarkonium than the D meson production. We have also found that $\Upsilon(1S)$ is more suppressed than B in our calculation, although it is not shown here.

3.4   Azimuthal angle correlation

Pair production of open heavy flavor covers wider kinematic region of the participating partons than quarkonium production. In this subsection we examine nuclear modification of the azimuthal angle correlation of the heavy meson pair $h\bar{h}$ in pA collisions [29, 39].

We define the azimuthal angle correlation between h and $\bar{h}$ as the pair-production multiplicity per event integrated over certain momentum and rapidity ranges with fixed
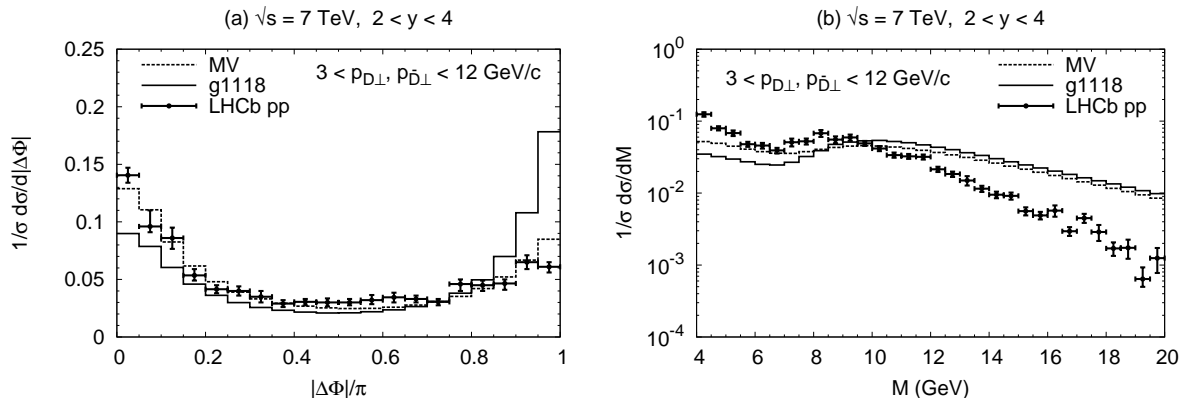
Figure 9: Azimuthal angle correlation (a) and invariant mass $M_{D\bar{D}}$ spectrum of $D^0\bar{D}^0$ pair production (b) in the rapidity and transverse momentum coverages, $2 < y_D, y_{\bar{D}} < 4$ and $3 < p_{D\perp}, p_{\bar{D}\perp} < 12\,\text{GeV}$ in pp collions at $\sqrt{s} = 7$ TeV, normalized by the total cross-section in the same fiducial region. For binning, $\Delta\Phi/\pi = 0.05$ in (a) and $\Delta M = 0.5$ GeV/c^2 in (b). Solid line denotes numerical result of Eq. (13) with uGD set g1118, the data points with error bars are taken from [19].

angle $\Delta\Phi$ between the pair:

$$CP[\Delta\Phi] = \frac{2\pi}{N_{\text{tot}}} \int p_{h\perp} dp_{h\perp}\, p_{\bar{h}\perp} dp_{\bar{h}\perp} dy_h dy_{\bar{h}} \frac{dN_{h\bar{h}}}{d^2\boldsymbol{p}_{h\perp} d^2\boldsymbol{p}_{\bar{h}\perp} dy_h dy_{\bar{h}}}, \qquad (17)$$

where N_{tot} is the pair multiplicity per event integrated over the same kinematic region and further integrated over the angle between the pair. The pair production cross-section of the heavy mesons is given in Eq. (13).

3.4.1 pp collisions

We compute the azimuthal angle correlation in $D^0\bar{D}^0$ pair production at the forward rapidity in pp collisions at $\sqrt{s} = 7$ TeV, using the uGD sets g1118 and MV. We use $m_c = 1.5$ GeV. In order to compare the result with LHCb data [19], we set the kinematical range as $2 < y_D, y_{\bar{D}} < 4$ and $3 < p_{D\perp}, p_{\bar{D}\perp} < 12\,\text{GeV}$, as plotted in Fig. 9 (a). In [19] the bin size of the azimuthal angle is chosen as $\Delta\Phi/\pi = 0.05$.

We immediately notice the near-side ($|\Delta\Phi| \sim 0$) and away-side ($|\Delta\Phi| \sim \pi$) enhancements in the numerical result. The away-side peak is naturally expected from the back-to-back kinematics of the LO quark-pair production from two gluons in the collinear factorization framework, but no near-side peak can be explained unless the higher-order processes are considered. In the CGC framework, on the other hand, gluon bremsstrahlung and multiple scatterings, which are encoded in $\phi_p^{q\bar{q},g}$, provide *intrinsic transverse momentum* $k_\perp \sim Q_s$ of incident gluons. This $k_\perp$ smears the away-side peak and generates the near-side peak in the angle correlation. In the LHCb data, indeed, we see the near-side peak but an only subtle away-side enhancement. The numerical result with set MV fairly

14

reproduces this LHCb angle correlation, whereas in the result with set g1118 the away-side peak still remains. This is presumably reflecting the fact that the uGD set MV has harder $k_\perp$ spectrum than set g1118. But one should recall that the uGD set MV is already disfavored in the global fit [27, 28] and in hadron production analysis at collider energies [30, 32].

The invariant mass spectrum of $D^0\bar{D}^0$ pair production in pp collisions at $\sqrt{s} = 7$ TeV is also measured in [19]. We compare in Fig. 9 (b) our numerical results with the data. The bin size for M is 0.5 GeV. The dip structure seen at low M is understood as the effect of the lower momentum cut at 3 GeV/c. Apparently the numerical result yields much harder invariant mass spectrum than the observed data.

Several remarks are here in order: First, large M pair production probes the gluons at large x_1, where as explained in Sec. 2 we extrapolate the uGD with a simple Ansatz (12), which is likely to overestimate the uGD in large x region and needs more refinement. Furthermore the back-to-back kinematics corresponds to the pair with the large M and small transverse momentum, where soft gluon emissions will be important and should be resummed [43]. Regarding small M pair on the near-side, full NLO extension of the pair production formula may be important although gluon splitting processes are partially included in the LO CGC formula (1).

3.4.2 pA collisions

Here we discuss modification of the azimuthal angle correlation between open heavy flavor meson (h) and open anti-flavor meson ($\bar{h}$) in pA collisions at $\sqrt{s} = 5.02$ TeV. We set the momentum coverage to $1 < p_{h\perp}, p_{\bar{h}\perp} < 5$ GeV.

In Fig. 10 (a) we plot the numerical result obtained with uGD set g1118 for the $D^0\bar{D}^0$ production at mid rapidity ($-1 < y < 0$). The away-side peak seen at $|\Delta\Phi| \sim \pi$ in pp collisions (initial scale Q_0^2) is gradually suppressed in pA collisions with increasing the (initial) saturation scale in the nucleus as $(4-6)Q_0^2$, while the near-side peak is slightly enhanced. This is due to the stronger multiple scatterings and saturation effects in the heavy nucleus. Then nuclear effects make $D^0\bar{D}^0$ correlation at low momentum closer to isotropic distribution. For comparison, we show the same plot but with the uGD set MV in Fig. 10 (b). Stronger enhancement of the correlation on the near side than on the away side is seen with increasing the saturation scale of the uGD in the nucleus. Different uGD sets result in quantitatively different correlation, but the qualitative features remain the same.

The nuclear modification of the angle correlation becomes more prominent in the forward rapidity region as seen in Fig. 10 (c). We have also computed the angle correlation in higher momentum region, $5 < p_{h,\bar{h}\perp} < 10$ GeV. We saw a strong away-side peak suppressed in pA collisions than in pp, while the near-side structure is unaffected. Note that the transverse momentum on the near side is provided solely by the intrinsic $k_\perp$ of the gluons in (15). The gluon saturation at $k_\perp \lesssim Q_s$ does not affect the particle production in such a high momentum region.

Finally, let us study $B^0\bar{B}^0$ correlations in the same kinematic region as $D^0\bar{D}^0$, to see
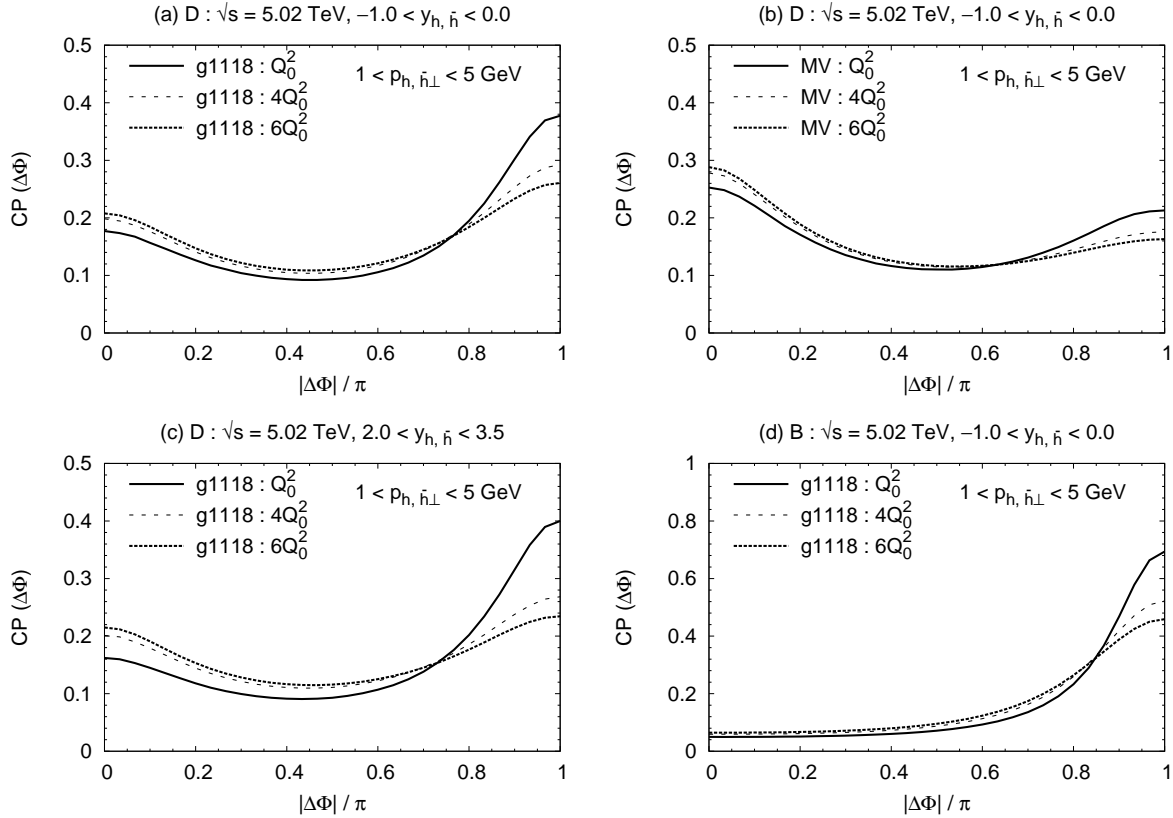
Figure 10: Nuclear modification of azimuthal angle correlation of heavy meson pair production in pA collision at $\sqrt{s} = 5.02$ TeV. Results with the initial saturation scale Q_0^2, $4Q_0^2$ and $6Q_0^2$ are plotted in solid, dashed and dotted lines, respectively. (a) $D^0\bar{D}^0$ correlation with set g1118 for $-1 < y_{h,\bar{h}} < 0$, (b) the same as (a) but with set MV, (c) the same as (b) but for $2 < y_{h,\bar{h}} < 3.5$, and (d) $B^0\bar{B}^0$ correlation with set g1118 for $-1 < y_{h,\bar{h}} < 0$. The momentum coverage is $1 < p_{h,\bar{h}\perp} < 5$ GeV, and $m_c = 1.5$ GeV for $D^0\bar{D}^0$ and $m_b = 4.8$ GeV for $B^0\bar{B}^0$.

the quark mass dependence of the correlation. As seen in Fig. 10 (d), despite that the momentum region is as low as in Fig. 10 (a), we do not confirm any correlation on the near side since intrinsic momentum of gluon is still insufficient to produce the pair there. The away-side peak exists and is suppressed with increasing $Q_{A,0}^2(x_0)$.

4 Summary

In this paper we have elaborated open heavy flavor meson production in high energy pA collisions at RHIC and LHC energies in the Color Glass Condensate framework. We have described the small-x gluon distribution in the heavy nucleus using the numerical solution of the rcBK equation which is constrained with the HERA DIS data.

At RHIC energy, D meson production proceeds from the moderate-x gluons, and there is not much room for x-evolution dynamics although its forward-rapidity production has marginal sensitivity to $x < x_0 = 0.01$. The nuclear modification factor R_{pA} of D shows a suppression at low $p_\perp$ and a Cronin-like enhancement at larger $p_\perp$ reflecting the multiple scattering effects implemented in the initial gluon distribution at $x = x_0$. In contrast, $R_{\mathrm{pA}}(p_\perp)$ of B is almost flat in $p_\perp$.

At LHC energy, D^0 production with constrained gluon distribution g1118 reasonably reproduces the $p_\perp$-dependence of the mid-rapidity data in pp collisions. The R_{pA} of D shows stronger suppression at low $p_\perp$ and no enhancement in computed $p_\perp$ region. The R_{pA} for $p_\perp$-integrated multiplicity shows a systematic suppression in the forward rapidity region, which is due to the quantum x-evolution effect of the gluons in the heavy nucleus. We have also compared the $R_{\mathrm{pA}}(y)$ of D with that of J/ψ computed in the color evaporation model, and found that J/ψ production is more suppressed. This is because the multiple scatterings additionally hinder the binding of the quark pair.

The B^0 production at the LHC is apparently overestimated by a factor than the data at forward rapidity. We notice that the production involves the large-x gluon distribution in the proton, which we parametrize with a simple Ansatz. Energy loss of the gluon in the nucleus may become also relevant there. The R_{pA} of B still shows a suppression with increasing rapidity y, but weaker than that of D.

As an unique candidate to study the gluon saturation in the nucleus, we have computed the azimuthal angle correlation for $D\bar{D}$ and $B\bar{B}$ pair in pp collision at LHC energy. Because of the finite $k_{1,2\perp}$ of the incident gluons, in addition to the away-side peak, the near-side peak emerges in $D\bar{D}$ correlation, which is also seen in LHCb data[19]. But we cannot quantitatively reproduce the angle correlation and the invariant mass spectrum of the data at the same time.

In order to see the saturation effect on the angle correlation qualitatively, we have calculated the $D^0\bar{D}^0$ correlation in pA collisions. We have found that the away-side peak is more smeared and the near-side peak is slightly enhanced for the larger saturation scale, i.e., with the heavier nucleus and/or at more forward rapidity. For $B\bar{B}$ correlation, we do not see the near-side peak because the saturation scale is not large enough to produce the $B\bar{B}$ in the same azimuthal direction.

Acknowledgments

Appendix : Cutoff $z_{\min}$

The lower limit of the z integration in Eq. (15) is given explicitly as

$$z_{\min} = \frac{q_{h\perp} \cosh y}{\sqrt{\frac{s}{4} - m^2 \cosh^2 y}} \; . \tag{18}$$

This can be readily derived by noting that the maximum energy of the produced quark and anti-quark in the center-of-mass frame is $E_q^{\max} = E_{\bar{q}}^{\max} = \frac{\sqrt{s}}{2}$. For the on-mass-shell quark, we have

$$E_q^{\max} = \sqrt{m^2 + (q_\perp^{\max})^2} \cosh y \; , \tag{19}$$

where y is the quark rapidity, which we set the same as the rapidity of the produced meson h. Then $z_{\min} \equiv q_{h\perp}/q_\perp^{\max}$ gives the desired expression.

References

[1] L. V. Gribov, E. M. Levin and M. G. Ryskin, Phys. Rept. **100**, 1 (1983).

[2] A. H. Mueller and J. -w. Qiu, Nucl. Phys. B **268**, 427 (1986).

[3] F. Gelis, E. Iancu, J. Jalilian-Marian and Raju Venugopalan, Ann. Rev. Nucl. Part. Sci. **60**, 463-489 (2010) [arXiv:1002.0333[hep-ph]].

[4] A.M. Stasto, K. Golec-Biernat, J. Kwiecinski, Phys. Rev. Lett. **86**, 596 (2001).

[5] F. Gelis, R. Peschanski, G. Soyez, L. Schoeffel, Phys. Lett. **B 647**, 376 (2007) [hep-ph/0610435].

[6] J.L.Albacete *et al.*, Int. J. Mod. Phys. E **22** (2013) 1330007 [arXiv:1301.3395 [hep-ph]].

[7] H. Fujii and K. Watanabe, Nucl. Phys. **A 915**, 1 (2013), [arXiv:1304.2221 [hep-ph]].

[8] J.P. Blaizot, F. Gelis, R. Venugopalan, Nucl. Phys. **A 743**, 57 (2004).

[9] H. Fujii, F. Gelis, R. Venugopalan, Nucl. Phys. **A 780**, 146 (2006).

[10] A. Adare, *et al.* (PHENIX Collaboration), Phys. Rev. C **84** (2011) 044905, [arXiv:1005.1627 [nucl-ex]].

[11] A. Adare, *et al.* (PHENIX Collaboration), Phys. Rev. C **86** (2012) 024909, [arXiv:1204.0754 [nucl-ex]].

[12] B. Abelev, *et al.* (ALICE Collaboration), JHEP 1209 (2012) 112, [arXiv:1203.2160 [nucl-ex]].

[13] B. Abelev, *et al.* (ALICE Collaboration), Phys. Rev. Lett.**109** (2012) 112301, [arXiv:1203.2160 [nucl-ex]].

[14] Y.L. Dokshitzer and D.E. Kharzeev, Phys. Lett. B **519**, 199 (2001).

[15] M. Djordjevic and M. Gyulassy, Nucl. Phys. A **733**, 265 (2004), [arXiv:0310.076 [nucl-th]].

[16] Y. Akamatsu, T. Hatsuda and T. Hirano, Phys. Rev. C **79**, 054907 (2009) [arXiv:0809.1499 [hep-ph]].

[17] V. Topor Pop, M. Gyulassy, J. Barrette, C. Gale, and M. Petrovici, [arXiv:1306.0885 [hep-ph]]

[18] R. Rapp and H. van Hees, R. C. Hwa, X.-N. Wang (Ed.) Quark Gluon Plasma 4, World Scientific, 111 (2010) [arXiv:0903.1096 [hep-ph]].

[19] R. Aaij, *et al.* (LHCb Collaboration), JHEP 1206 (2012) 141 [arXiv:1205.0975 [hep-ex]].

[20] R.Maciula and A.Szczurek, Phys. Rev. D **87** (2013) 094022 [arXiv:1301.3033 [hep-ph]].

[21] M. Nahrgang, J. Aichelin, P.B. Gossiaux and K. Werner, arXiv:1305.3823 [hep-ph].

[22] I. Balitsky, Nucl. Phys. **B 463**, 99 (1996).

[23] Yu.V. Kovchegov, Phys. Rev. **D 54**, 5463 (1996).

[24] I. Balitsky, Phys. Rev. D **75**, 014001 (2007).

[25] J.L. Albacete, Yuri V. Kovchegov, Phys. Rev. **D** 75, 125021 (2007) [arXiv:0704.0612[hep-ph]].

[26] J.L. Albacete, Phys. Rev. Lett. **99**, 262301 (2007) [arXiv:0707.2545 [hep-ph]].

[27] J.L. Albacete, Nestor Armesto, J.G. Milhano, C.A. Salgado, Phys. Rev. D **80**, 034031 (2009) [arXiv:0902.1112[hep-ph]].

[28] J.L. Albacete, N. Armesto, J.G. Milhano, P. Quiroga-Arias, and C.A. Salgado, Eur. Phys. J. C **71**, 1705 (2011) [arXiv:1012.4408[hep-ph]].

[29] J.L. Albacete and C. Marquet, Phys. Rev. Lett.**105** (2010) 162301 [arXiv:1005.4065 [hep-ph]].

[30] J. L. ALbacete and A. Dumitru, arXiv:1011.5161 [hep-ph].

[31] H. Fujii, K. Itakura, Y. Kitadono and Y. Nara, J. Phys. G **38**, 124125 (2011) [arXiv:1107.1333 [hep-ph]].

[32] J. L. Albacete, A. Dumitru, H. Fujii and Y. Nara, Nucl. Phys. A **897**, 1 (2013) [arXiv:1209.2001 [hep-ph]].

[33] V.G. Kartvelishvili, A.K. Likhoded and V.A. Petrov, Phys. Lett. **B 78**, 615 (1978).

[34] F.D. Aaron *et al.* (H1 Collaboration), Eur. Phys. J. **C59**, 589 (2009).

[35] J.Abdallah *et al.* (DELPHI Collaboration), Eur. Phys. J. **C 71**, 1557 (2011) [arXiv:1102.4748 [hep-ex]].

[36] see Particle Data Group (http://pdg.lbl.gov/2008/reviews/rpp2008-rev-frag-functions.pdf).

[37] J.Abdallah et al. (DELPHI Collaboration), [hep-ex/0311005].

[38] B. Abelev, *et al.* (ALICE Collaboration), JHEP 1201 (2012) 128, [arXiv:1111.1553 [hep-ex]].

[39] K. Dusling and R. Venugopalan, Phys. Rev. D**87** (2013) 094034, [arXiv:1302.7018 [hep-ph]].

[40] L.Adamczyk et al. (STAR Collaboration), Phys. Rev. D **86** (2012) 072013, [arXiv:1204.4244 [nucl-ex]].

[41] J.Adams et al. (STAR Collaboration), Phys. Rev. Lett.**94** (2005) 062301, [arXiv:nucl-ex/0407006].

[42] R. Aaij *et al.* (LHCb Collaboration), [arXiv:1306.3663 [hep-ex]].

[43] A. H. Mueller, B.-W. Xiao and F. Yuan, Phys. Rev. Lett.**110** (2013) 082301, [arXiv:1210.5792 [hep-ph]].